Novel thermal management methods to improve the performance of the Li-ion batteries in high discharge current applications

Hamidreza Behi [a, b, *], Danial Karimi [a, b], Joris Jaguemont [a, b], Foad Heidari Gandoman [a, b], Theodoros Kalogiannis [a, b], Maitane Berecibar [a, b], Joeri Van Mierlo [a, b]

[a] Research Group MOBI — Mobility, Logistics, And Automotive Technology Research Centre, Vrije Universiteit Brussel, Pleinlaan 2, Brussels, 1050, Belgium
[b] Flanders Make, Heverlee, 3001, Belgium

ARTICLE INFO

ABSTRACT

Over the last few decades investigating the performance of thermal management in the high charge/ discharge current has been taken into consideration in many studies. In this study, a mature heat pipe-based air cooling system is built to control the temperature of the lithium-ion (Li-ion) cell/module in the high current (184 A) discharging rate. The temperature of the cell/module experimentally and numeri-cally is considered by the lack of natural convection, natural convection, forced convection, and evap-orative cooling. According to the experimental results, the natural and forced convection decrease the average temperature of the cell by 6.2% and 33.7% respectively. Moreover, several numerical simulations are solved by COMSOL Multiphysics®, the commercial computational fluid dynamics (CFD) software. The simulation results are validated against experimental results at the cell level for natural and forced convection. It indicates that the evaporative cooling method is robust to enhance the current cooling system method for further optimization. The results show that there is a 35.8% and 23.8% reduction in the maximum temperature of the cell and module due to the effect of the evaporative cooling method respectively.

© 2021 The Author(s). Published by Elsevier Ltd. This is an open access article under the CC BY license (http://creativecommons.org/licenses/by/4.0/).

1. Introduction

Nowadays, the transportation system consumes a lot of fuel, which leads to global warming, energy shortage, and environ-mental pollution as serious problems for human life. Thus, electric vehicles (EVs) have received worldwide attention in recent years due to the expected energy shortage and environmental pollution problems. Recently, lithium-ion (Li-ion) batteries have become more popular among all kinds of power batteries because of their low self-discharge rate, environmental friendliness, high energy density, long life cycle, and high voltage, which is an appropriate energy storage solution in EVs applications [1–5]. Nevertheless, the energy density, capacity, efficiency, and cycling life of Li-ion bat-teries are highly dependent on their thermal management [6,7]. Generally, Li-ion batteries in the temperature range of 25 °C–40 °C have the best performance [8,9]. Conventional battery technology

supports charging/discharging at relatively low current applica-tions. However, a high current is necessary when vehicles climb the hills or during fast charging. As a noticeable amount of heat generated within the Li-ion batteries in high current applications, define and design an appropriate thermal management system is essential.

It has been investigated by many researchers that active and passive cooling systems such as liquid cooling, air cooling, phase change materials (PCMs), and heat pipe can control the tempera-ture rising and improve the stability of electronic devices and Li-ion batteries in charging/discharging process [10–16]. Liquid coolants have a high heat transfer coefficient, which makes them an oper-ative, efficient, quiet, and compact cooling medium. The liquid cooling system, as a promising cooling system, has been used by many researchers [17–20]. However, liquid cooling systems have a massive and complex structure with high investment costs and power consumption. Usage components like liquids, pumps/com-pressors, and tubing increase the weight of the system and leakage risk [21]. Air cooling is an active cooling system with a simple structure, low cost, easy maintenance, and lightweight, which is used in many cooling applications [22–24]. Nonetheless, due to the

* Corresponding author. Research Group MOBI — Mobility, Logistics, And Auto-motive Technology Research Centre, Vrije Universiteit Brussel, Pleinlaan 2, Brussels, 1050, Belgium.
E-mail address: hamidreza.behi@vub.ac.be (H. Behi).

Nomenclature

Δt	Time Interval (t)
T	Battery Temperature (K)
I	Discharge Current (Ah)
V	Operating Voltage (V)
V_{oc}	Open-circuit Voltage
m	Mass of the Cell (kg)
c_p	Specific Heat Capacity (J/kg.K)
T_{amb}	Ambient Temperature (K)
R_{bt}	Total Resistance of the Battery (K/W)
R_{tab}	Total Resistance of the Battery Tab (K/W)
R_0	Ohmic Resistance
k	Thermal Conductivity (W/m.K)
p	Pressure (Pa)
S	Cross-section of the Tab and Cell (m^2)
h	Heat Transfer Coefficient (W/m^2.K)
q_{conv}	Free Cooling Heat Transfer (W)
Q_{Cell}	Power Loss of Battery (W)
g_i	Gravity (m/s^2)
Q_{hp}	Heat Transferred by Heat pipe (W)
q_g	Cell Heat Generation (W)
V	Volume (m)
H	Height (m)
v	Kinematic Viscosity (m^2/s)
h_{vs}	Enthalpy of Water Vapor at Water Surface Temperature (J/kg)
W_{asw}	Humidity Ratio of Air (kg$_{water}$/kg$_{dry\ air}$)

h_a	Enthalpy of the Air (W/m^2.K)
K_1	Mass Transfer Coefficient (Kg/m^2.s)
K	Evaporation Rate
M_V	Molar Mass of Water Vapor
c_V	Vapor
c_{sat}	Saturation Concentration

Greek

α	Thermal Diffusivity (m^2/s)
β	Thermal Expansion (1/K)
ρ	Density (kg/m^3)
ρ'	Resistivity (K/W)
ν	Velocity (m/s)

Acronyms

CFD	Computational Fluid Dynamics
TMS	Thermal Management System
Li-ion	Lithium-ion
PCM	Phase Change Material
EV	Electric Vehicles
Nu	Nusselt Number
Pr	Prandtl Number
Ra	Rayleigh Number
HPPC	Hybrid Pulse Power Characterization
SOC	State of Charge
Sec	Second
ECM	Electric-Equivalent-Circuit
WLTC	World Harmonized Light Vehicle Test Procedure

low heat transfer coefficient and heat capacity of air, such cooling systems hardly control the battery's cell/module temperature in a safe range in high current applications [25]. PCM is a passive cooling system that has been using by researchers in many cooling and energy storage applications [26–29]. As PCMs suffer from low-thermal conductivity, several studies have been done to improve PCMs thermal conductivity by adding Nanomaterial, graphite, Nanocarbon tube, aluminum mesh, etc. [30–33]. However, leaking issues, low thermal stability, high cost, and limited temperature range of phase change has influenced the usage of the PCMs. The heat pipe is an efficient passive heat transfer device in which heat can be transferred efficiently at a high rate with a very low-temperature drop in a specified length. Many researchers have been using the heat pipe for battery cooling [34–36]. Feng et al. [36] experimentally examined the thermal and strain management for the cylindrical battery pack at a 0.5–1C rate using heat pipe and air cooling. They found a heat pipe air cooling system in the center of the battery pack is an ideal TMS through a number of tests. Behi et al. [37] numerically considered the effect of the heat pipe with copper sheets (HPCS) on the cylindrical battery module at a 1.5C discharging rate. They found the maximum module temperature in different cooling scenarios comprising forced-air cooling, heat pipe, and HPCS decreased by up to 34.5%, 42.1%, and 42.7%, respectively. Dan et al. [38] experimentally and numerically investigated the micro heat pipe array-air battery cooling for a prismatic battery pack. They found an air velocity of 3 m/s can control and preserve the heat dissipation of the battery pack under the 3C discharging rate. Zhao et al. [39] experimentally investigated the heat pipe-based wet cooling system to control the Li-ion prismatic battery pack under a 3C discharging rate. They found that a combination of forced convection and wet cooling approaches can control the temperature of the battery pack in a suitable temperature range with the least cost of energy and water spray. Tran et al. [40] experimentally considered the feasibility of the flat heat pipe air cooling system for the cylindrical battery module. They found a flat heat pipe operates more efficiently compared with a conventional heat sink and kept the module temperature under 50 °C. Zhao et al. [41] experimentally considered the effect of a direct evaporative cooling approach for the cylindrical battery module. They proved that the evaporative cooling approach is a capable method to control the maximum cell temperatures, temperature differences, and capacity fading of batteries.

The mentioned relevant studies shown the superior thermal performance of heat pipe based air-cooled systems in battery TMS, in module/pack level. However, all of the existing studies were carried out in low currents and normal conditions as air cooling is not practical in high current applications due to the lack of air heat transfer coefficient. In the current study, several capable and mature heat pipe-based air cooling technology is investigated to control the temperature of an LTO cell/module during an 8C discharging rate (184 A). The suggested charging/discharging current rate of the LTO cell is from 4.6 A to 92 A. Nevertheless, in the present study, the temperature distribution of the cell is studied at a184 A at the maximum current rate. The experimental tests are done to investigate the effect of natural and forced convection on the cell level. A CFD model for forced convection is validated with the experimental results and attained an acceptable agreement. As an optimization, the effect of natural and forced convection is considered on the module level consisting of the 30 cells. Moreover, the effect of evaporative cooling as a developing cooling method in

the ability to dissipate high heat flux at reasonable energy is considered. The heat generated from the cell/module is absorbed by water evaporation through the assist of heat pipes. The results show a consistent and successful cooling procedure from the natural convection to evaporative cooling at the cell/module level. The paper is prepared as follows. Section 2 represents the experimental setup. In Section 3, the experimental results of natural and forced convection are presented. The numerical and thermal modeling, validation, and optimization of the battery cell/module model are described in Section 4. The performance of the thermal management methods at the module level is presented in section 5. A comparison of the proposed cooling systems in the cell and module levels is described in section 6. Lastly, a relevant conclusion is drawn in section 7.

2. The objective of the research and requirements

2.1. Objective of the research

The temperature rise in Li-ion battery cells, especially at high current applications leads to capacity fade and thermal runaway of the cells. Using an air cooling system for high current applications need an appropriate and developed design to control the maximum battery's cell/module temperature in a safe range (25–40 °C). The importance of a cooling system will be more revealed in the module when the cells are closely packed. The design of the current heat pipe based air cooling system is selected for developing a more successful cooling system based on the review of previous works. In the current study, the hybrid cooling system is investigated
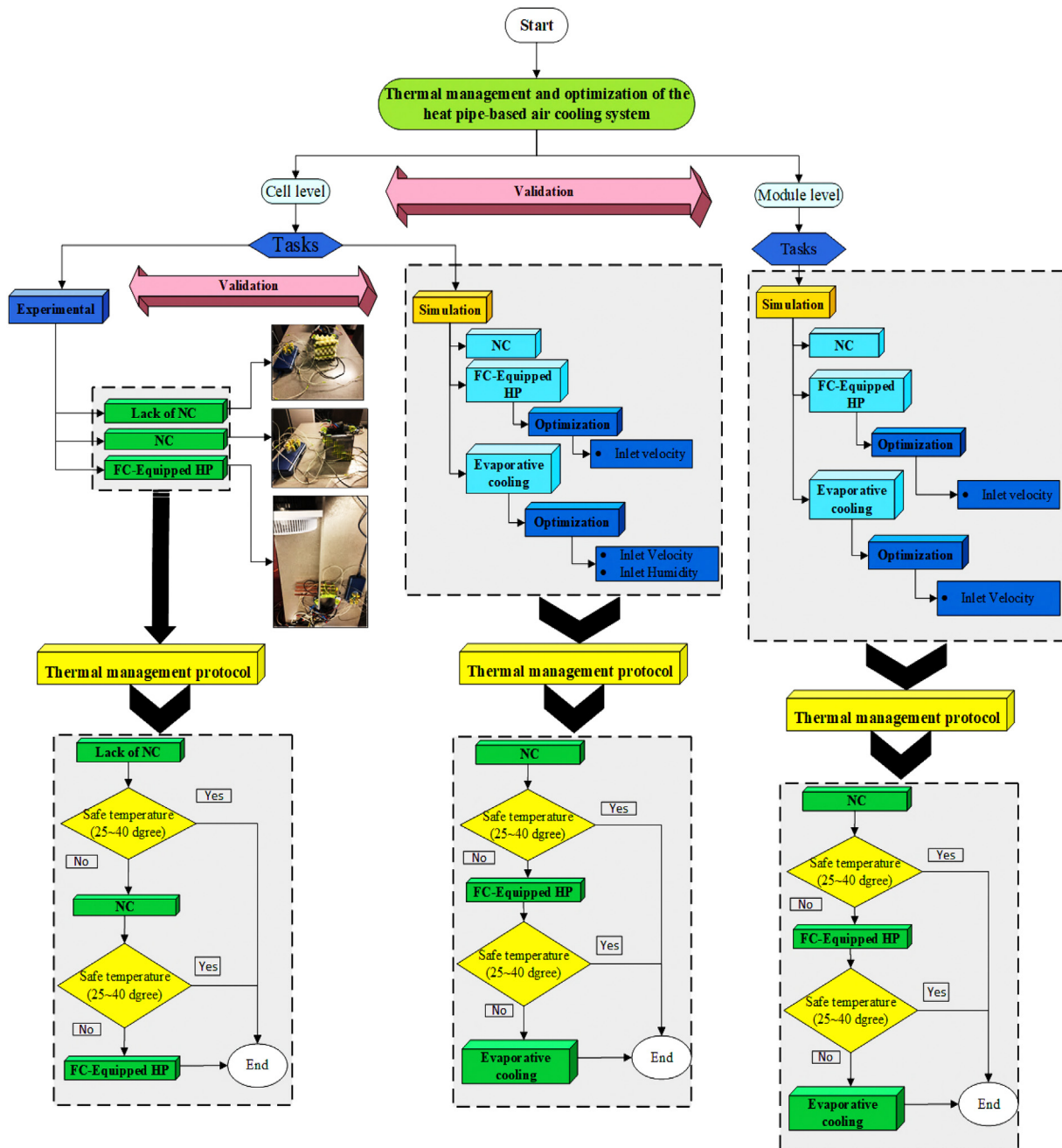

Fig. 1. The experimental and simulation flowchart (NC: Natural convection, FC: Forced convection, HP: Heat pipe).
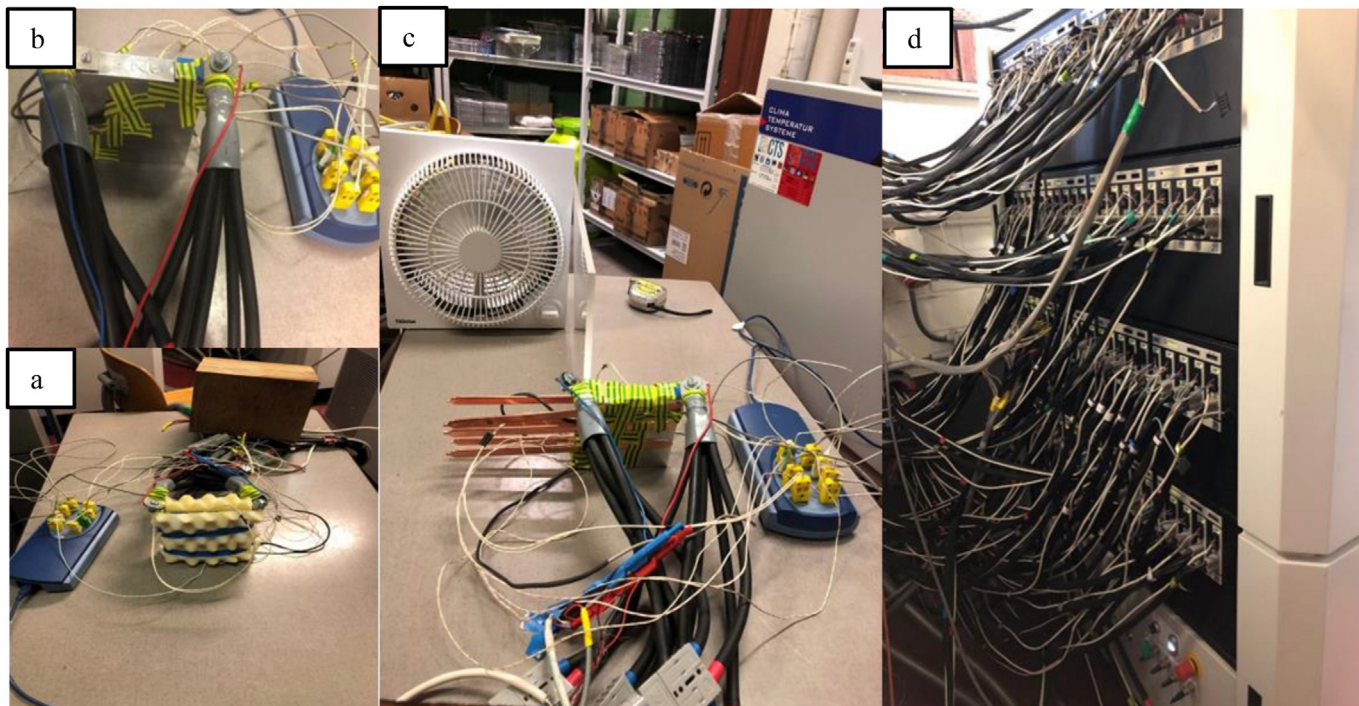
Fig. 2. The component and setup of, (a) lack of natural convection, (b) natural convection, (c) forced convection, (d) battery tester, and (e) the schematic of the test setup.

experimentally and numerically. In experimental tests, the temperature of the cell is investigated in the lack and presence of

Fig. 3. The heat transfer mechanism in heat pipe [29].

natural convection. Moreover, the effect of heat pipe forced convection is considered on the cell temperature. The CFD model is developed using COMSOL Multiphysics and validates with experimental results for further consideration. The effect of natural convection, force convection, and evaporative cooling is simulated with various optimizations, such as the different inlet velocity and humidity, inlet, and outlet location at the cell/module level. The applied designs have changed air cooling as a promising cooling system to control the temperature rise of the cell/module in high current applications. The effect of the air cooling and heat pipe for the Li-ion battery cell/module is considered in various studies. However, there are a few studies to investigate the effect of air-cooling, heat pipe, and evaporative cooling for high current applications. Fig. 1 shows the whole experimentation, simulation, and
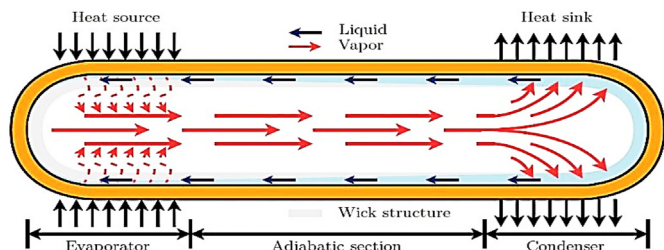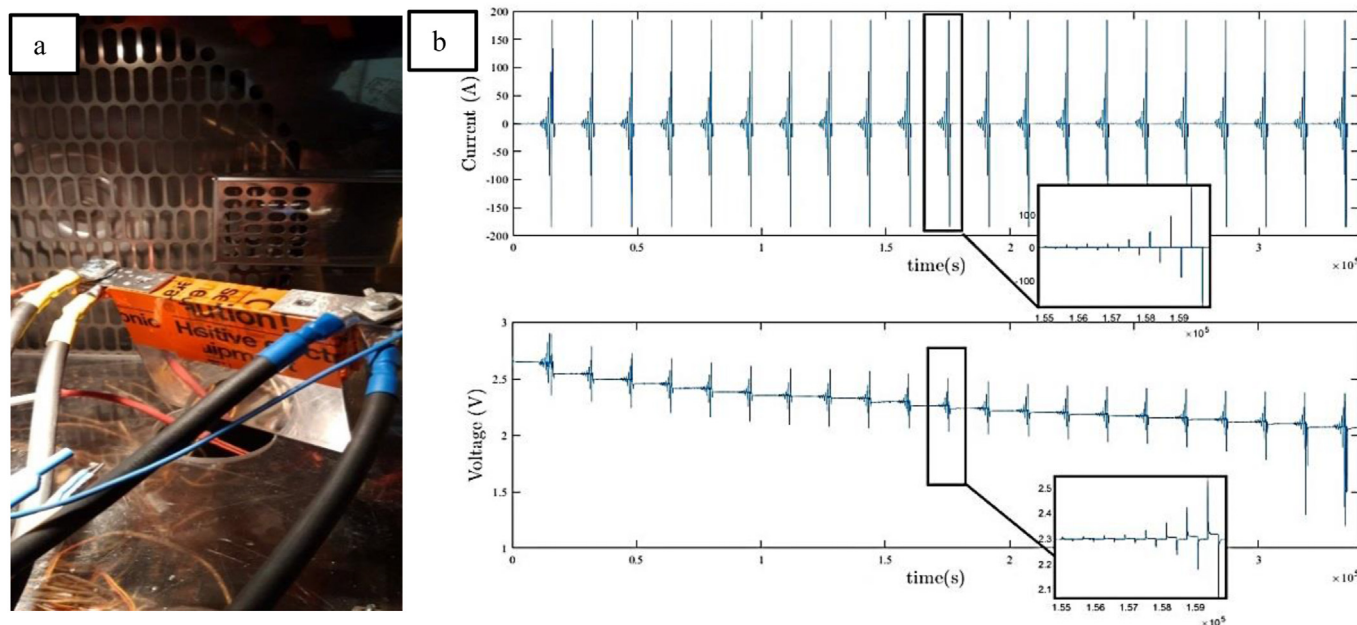
Fig. 4. (a) The LTO cell under the HPPC test in the climate chamber at 25 °C and (b) the result of the HPPC test.

Table 1
The uncertainties of the experimental parameters.

Parameter	Uncertainty
Current (A)	±0.005
Voltage (V)	±0.005
Thermocouple (°C)	±0.2
Data logger (°C)	±0.025

optimization which are carried out in the flowchart.

2.2. Requirements

Fig. 2 displays the experimental setup of the LTO cell in lack of natural convection, presence of natural convection, and heat pipe-based air cooling system. The test setup consists of an LTO cell, six flat heat pipes, a cooling fan, a data logger, eight K-type thermocouples, an anemometer, a PEC battery tester, a thermal camera, and a personal computer. The battery tester is a PEC ACT0550 which is capable of supplying up to 5 V DC and 50 A per channel with a ±0.005 accuracy. The charging/discharge cycles, voltage, and current are controlled and recorded by the battery tester while the K-type thermocouples measure the temperature data from the cell. All the thermocouples are calibrated with a maximum tolerance of ±0.2 °C. It is essential to mention that the ambient room temperature is fixed at 22 °C. The discharging tests are done at 8C with a high current rate of 184 A in a 446-sec current profile.

The LTO prismatic cell (L 22 mm × H 103 mm × W 115 mm) has a nominal capacity of 23 Ah and a rated voltage of 2.3 V, as shown in Fig. 2. The flat heat pipe (L 3.5 mm × H 250 mm × W 11.2 mm) is made of copper with a sintered wick structure and distilled water as a working fluid. The thermal conductivity of the heat pipes is calculated experimentally at 8212 W/m.K [42]. With the aim of a uniform and capable cooling system, six heat pipes are connected to both sides of the cell. In order to reduce the thermal contact resistance, a thin layer of gap filler with thermal conductivity of 8 W/m.K is applied at the interfaces between the cell and the heat pipes. According to Fig. 3, the heat generation inside the cell and
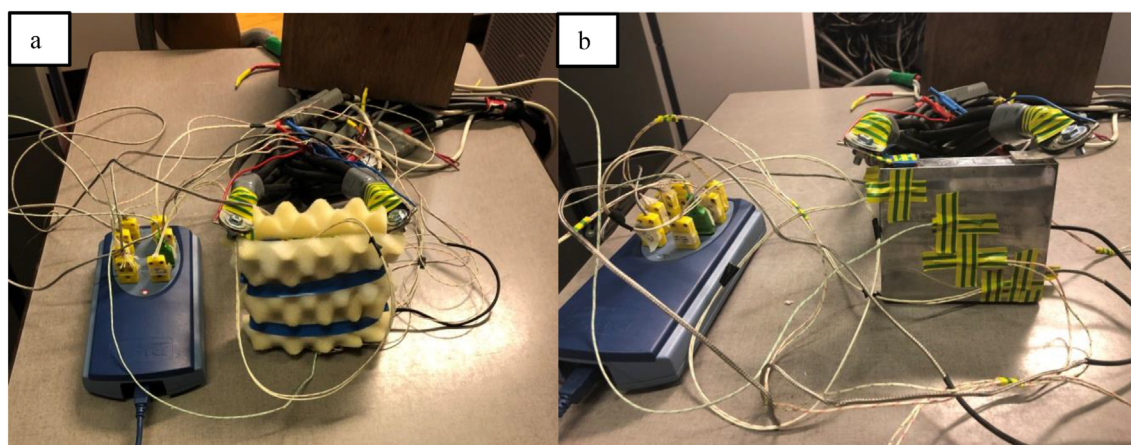

Fig. 5. (a) The picture of the LTO cell in the lack of the natural convection and (b) presence of natural convection.
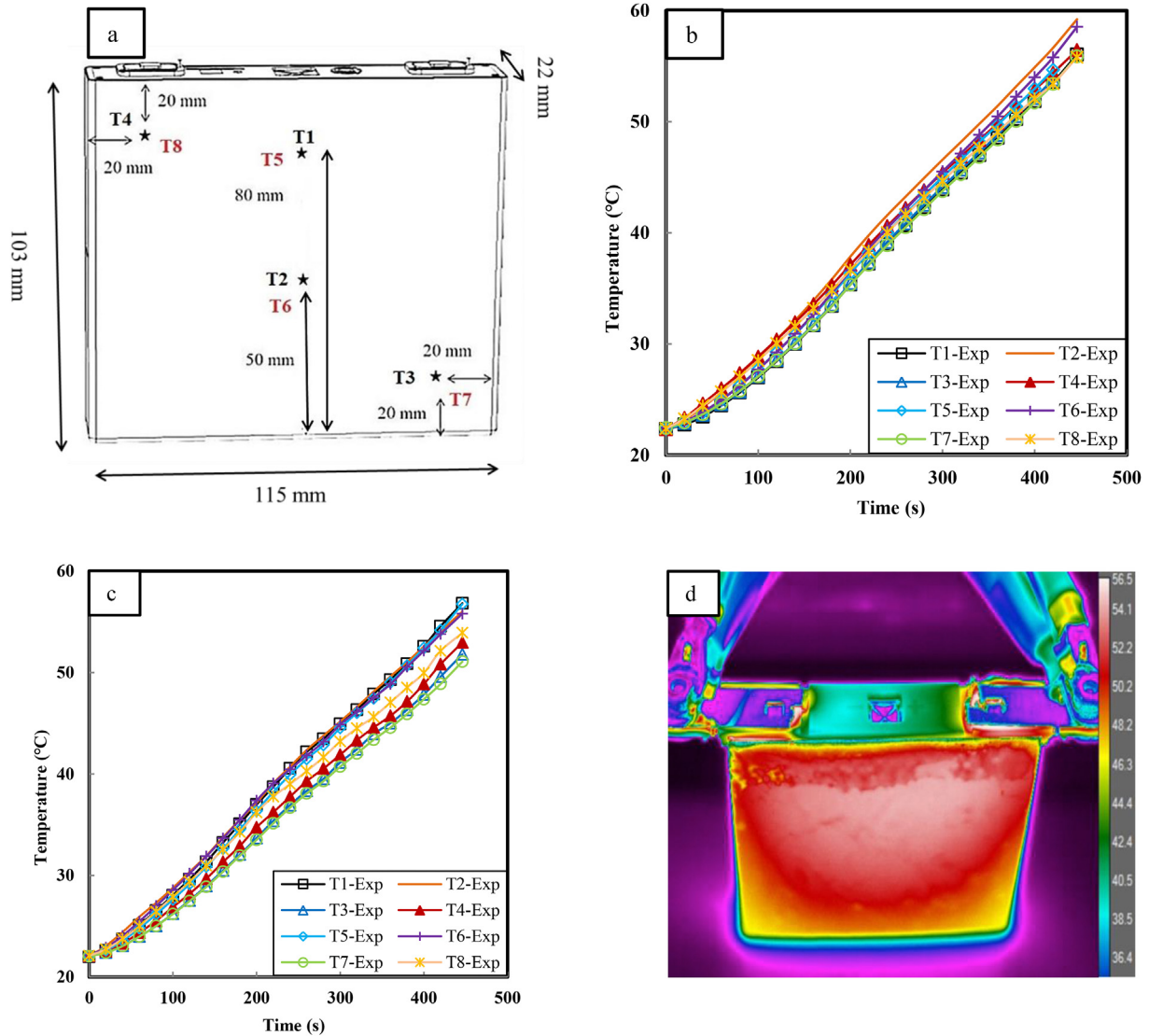
Fig. 6. (a) Location of thermocouples of the front (T$_1$-T$_4$) and backside (T$_5$-T$_8$) of the cell, (b) temperature of the cell in lack of natural convection, (c) the temperature of the cell, and (d) thermal image in the presence of natural convection (Exp: Experiment).

tabs in the discharging process is transferred by the evaporator sections of the heat pipes to the condenser sections and from there by natural/forced convection to the cooling medium. The condensed working fluid returns by capillary force to the evaporator section in the wick structure.

Measuring the internal resistance of the battery is the key parameter to calculate the heat generation of the battery in the CFD model of the battery. The hybrid pulse power characterization (HPPC) test is intended to measure the battery's internal resistance using a test profile that incorporates both discharge and charge pulses. The primary objective of this test is to establish, as a function of the SOC, the current rate, and the DC internal resistance of the three tested cells. The idea of this test is to apply a 10-s discharge-pulse and 10-s charge-pulse power capabilities at each given SOC and for different C-rates. A 600s-rest period is scheduled between each HPPC pulse. From the data, an algorithm will afterward determine the DC internal resistance of the cell. Fig. 4a and b depicts the cell under the HPPC test in the climate chamber at 25 °C and the result of the test, respectively.

Equation (1) displays the Schultz and Cole [43,44] method to calculate the uncertainty.

$$U_R = \left[\sum_{i=1}^{n} \left(\frac{\partial R}{\partial V_I} U_{VI} \right)^2 \right]^{1/2} \tag{1}$$

Where U_{VI} and U_R are the error of each factor and total errors respectively. The measurement correctness of each factor is shown in Table 1. The maximum uncertainty is calculated as 2.01%.

3. Experimental results in the cell level

3.1. Investigation of lack of natural convection and natural convection cooling system

The first phase of the experiment is conducted under the condition of the lack of natural convection and natural convection at the discharge rate of 8C and the ambient temperature of 22 °C. Natural convection has a direct effect on the operating temperatures of the battery and electronic devices. Natural convection is the initial step of temperature distributions within the battery cell/
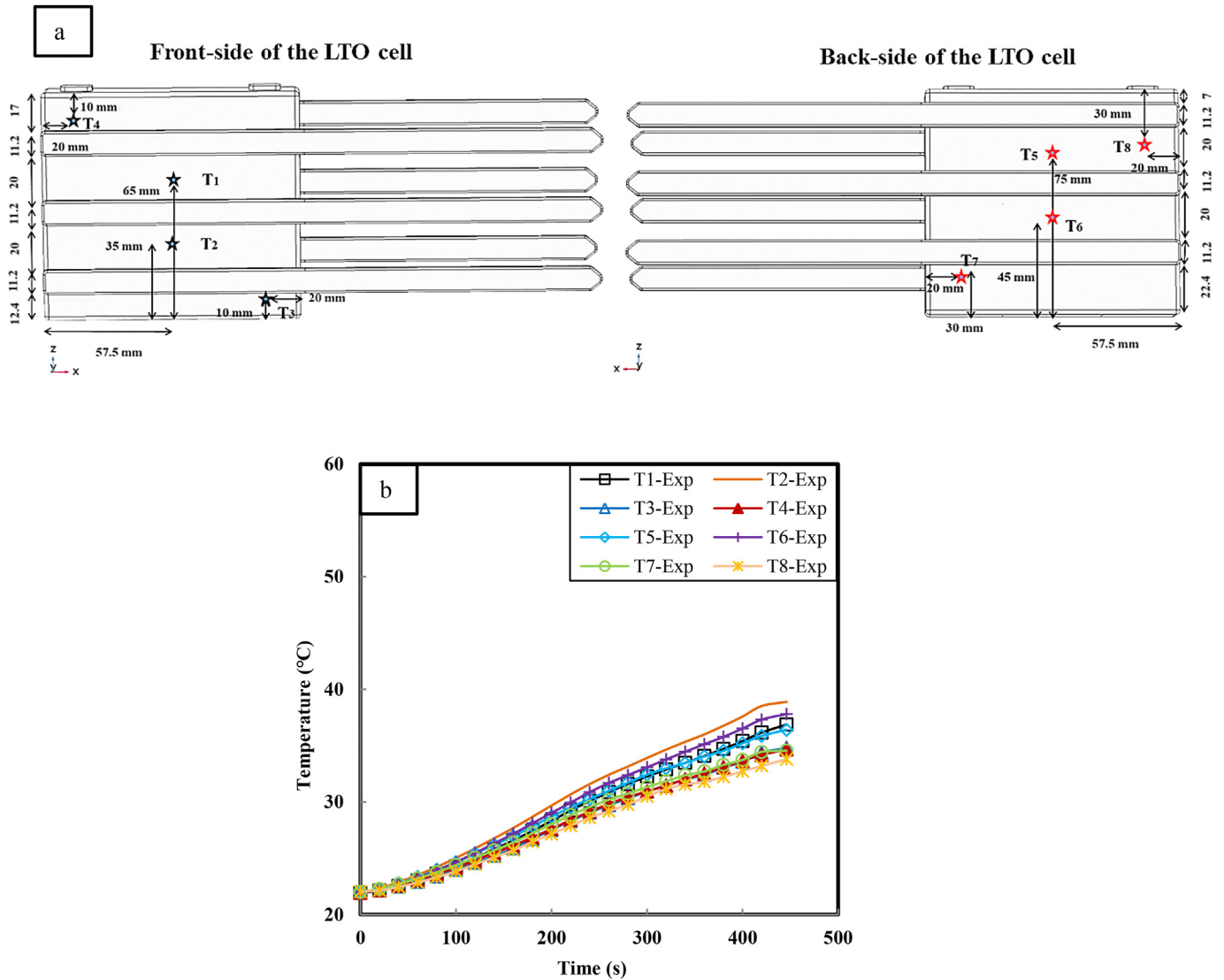
Fig. 7. (a) The schematic front and back-side of the cell, and (b) the temperature of the cell in the presence of forced convection and six flat heat pipes.
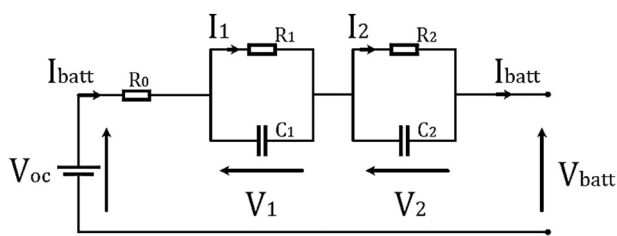

Fig. 8. Equivalent impedance model of the LTO prismatic cell.

module in determining heat losses. In natural convection, buoyancy forces cause the fluid motion inside the fluid, whereas, in forced convection, there is an external force. Fig. 5 shows the experimental test setup for LTO cell under the lack of natural convection and natural convection. It is necessary to mention that the whole surface of the cell is insulated precisely to prevent the cooling effect of natural convection.

As it is approved to preserve the best performance and to reach the full lifespan of the battery cells, the temperatures of all the cells must be kept between 25 and 40 °C [8]. If the natural convection

performs an efficient cooling, there is no need for other kinds of cooling strategies. Fig. 6 shows the location of thermocouples, the temperature of the cell in lack of natural convection, natural convection, and thermal image of the LTO cell during the discharging process.

It is evident in Fig. 6c that the natural convection has a slight effect on the temperature of the cell. The average temperature of the cell in the lack of natural convection reached 57.9 °C (Fig. 6b). On the other hand, the average temperature of the cell in the presence of the natural convection reached 54.3 °C, which shows a 6.2% reduction. In order to compute the heat transfer coefficient for natural convection, the average temperature (film temperature) of the cell and ambient air is calculated. The Rayleigh number is calculated as follows [45]:

$$Ra = \frac{g\beta(T_s - T_\infty)L^3}{\alpha v} \tag{2}$$

where g, β, L, α, and v are body force, volumetric thermal expansion coefficient, height, thermal diffusivity, and kinematic viscosity, respectively. By the estimation of air as an ideal gas, the Rayleigh number is calculated at $1.34 \times e6$. The Nusselt number has been
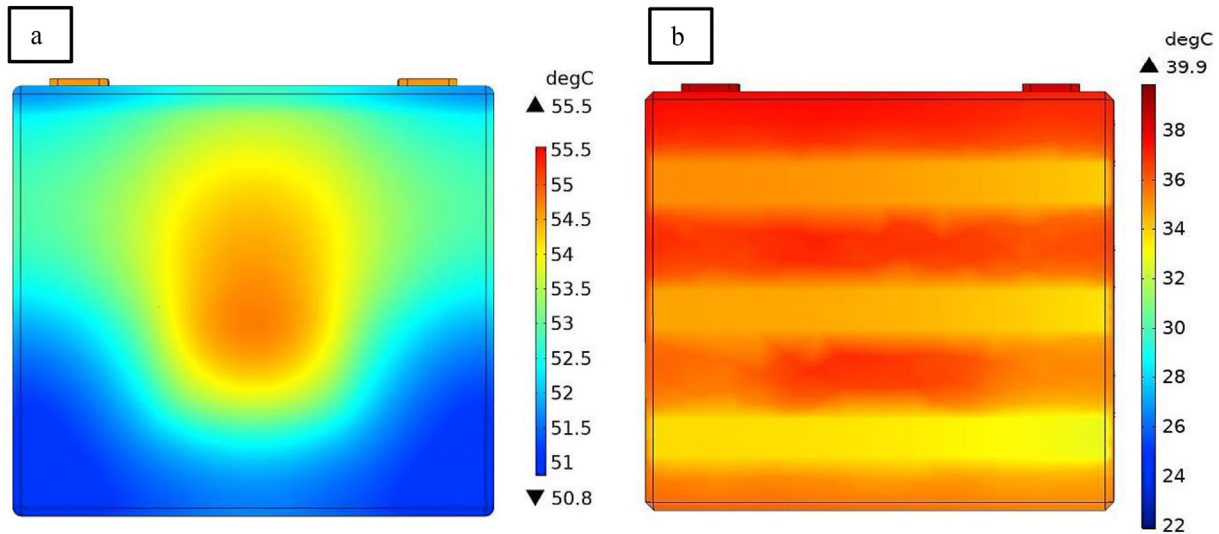
Fig. 9. (a) Temperature contour of the LTO cell in (a) natural convection and (b) forced convection.

calculated based on equation (3):

$$\text{Nu} = \left(0.825 + \frac{0.387 Ra^{1/6}}{\left[1 + \left(\frac{0.492}{Pr} \right)^{\frac{9}{16}} \right]^{8/27}} \right)^2 \quad (3)$$

where the Pr stands for Prandtl number. According to equation (3), the value of the Nusselt number is calculated at 26.94. Finally, the heat transfer coefficient calculated 6.87 W/m^2. K as follows:

$$h = \frac{\text{Nu} \times \text{k}}{L} \quad (4)$$

where k is the thermal conductivity of air at the film temperature.

3.2. Investigation of forced convection

Forced convection cooling system is one of the most commonly used active cooling methods due to its low cost of maintenance, manufacturing, and simplicity. In the current study, a forced convection cooling system is selected to control an appropriate temperature range for the LTO cell. The cell is equipped with six flat heat pipes to keep the uniform temperature distribution inside the cell. Since there is a non-uniform temperature distribution inside the cell, the location of heat pipes has been chosen in a way to reach better temperature uniformity. The ambient temperature and inlet velocity are set at 22 °C and 3 m/s, respectively. The power consumption of the fan is reported 12 W at 3 m/s.

Fig. 7 shows the effect of the forced convection cooling system for thermal management of an LTO cell. The average temperature of the cell equipped with heat pipes in the presence of the forced convection reached 35.97 °C, which shows a 33.7% reduction compare with the natural convection cooling method.

4. Numerical modeling based on experimental results

4.1. Thermal modeling

With the purpose of thermal modeling, a combination of Matlab/Simulink with COMSOL Multiphysics is used. The internal heat source of the battery cell is generated due to ohmic resistance and is

provided by Matlab/Simulink. For this purpose, an electrical model of the LTO prismatic cell is generated and validated according to the dual-polarization electric-equivalent-circuit (ECM) approach [46]. The model consists of the open-circuit voltage (V_{oc}) and the series-connected ohmic resistance R_0 as well as two parallel R//C branches which represent the time-dependent polarization processes that take place at an applied potential to the battery terminals (V_{batt}). Fig. 8 shows the proposed impedance model that is used in this study.

In order to obtain the parameters of the proposed ECM, several characterization experiments are conducted. Starting from the precondition and the discharge capacity tests, the capacity at various discharge current rates is obtained. The HPPC is then performed to derive the voltage response of the battery cell at various current rates. A sequence of eight current pulses (C/5, C/4, C/3, C/2, 1C, 2C, 4C, 8C) with 10-sec duration is injected into the LTO cell during both charge and discharge, over the whole operating voltage with a 5% SOC step. The mathematical model formulation in order to parameterize the proposed ECM can be found in Ref. [46]. The open-circuit voltage test is also performed to investigate the V_{oc} at a predefined ambient temperature. The model is validated with the world harmonized light vehicle test procedure (WLTC) and the heat generation of the LTO cell is obtained by considering the Joule losses.

$$q_g R_0 . I_{batt}{}^2 + R_1 . I_1{}^2 + R_2 . I_2{}^2 \quad (5)$$

In the direction of the explanation of the transient thermal distribution in the LTO cell, an energy balance equation is used. According to this equation, the thermal energy which is produced inside the cell or is transferred its surrounding is formulated as equation (6):

$$mC_p \frac{\partial T}{\partial t} + q_{conv} = k_x \frac{\partial^2 T}{\partial x^2} + k_y \frac{\partial^2 T}{\partial y^2} + k_z \frac{\partial^2 T}{\partial z^2} + q_g \quad (6)$$

where q_g and T describe the heat generation and cell temperature, respectively. C_p, k, and m are the specific heat capacity, the thermal conductivity along (x,y,z)-axis, and mass of the cell respectively. Also, the external heat source of the battery cell is generated by tab domains because of the resistive loss. The transient thermal distribution of the tabs are derived as follows [42]:
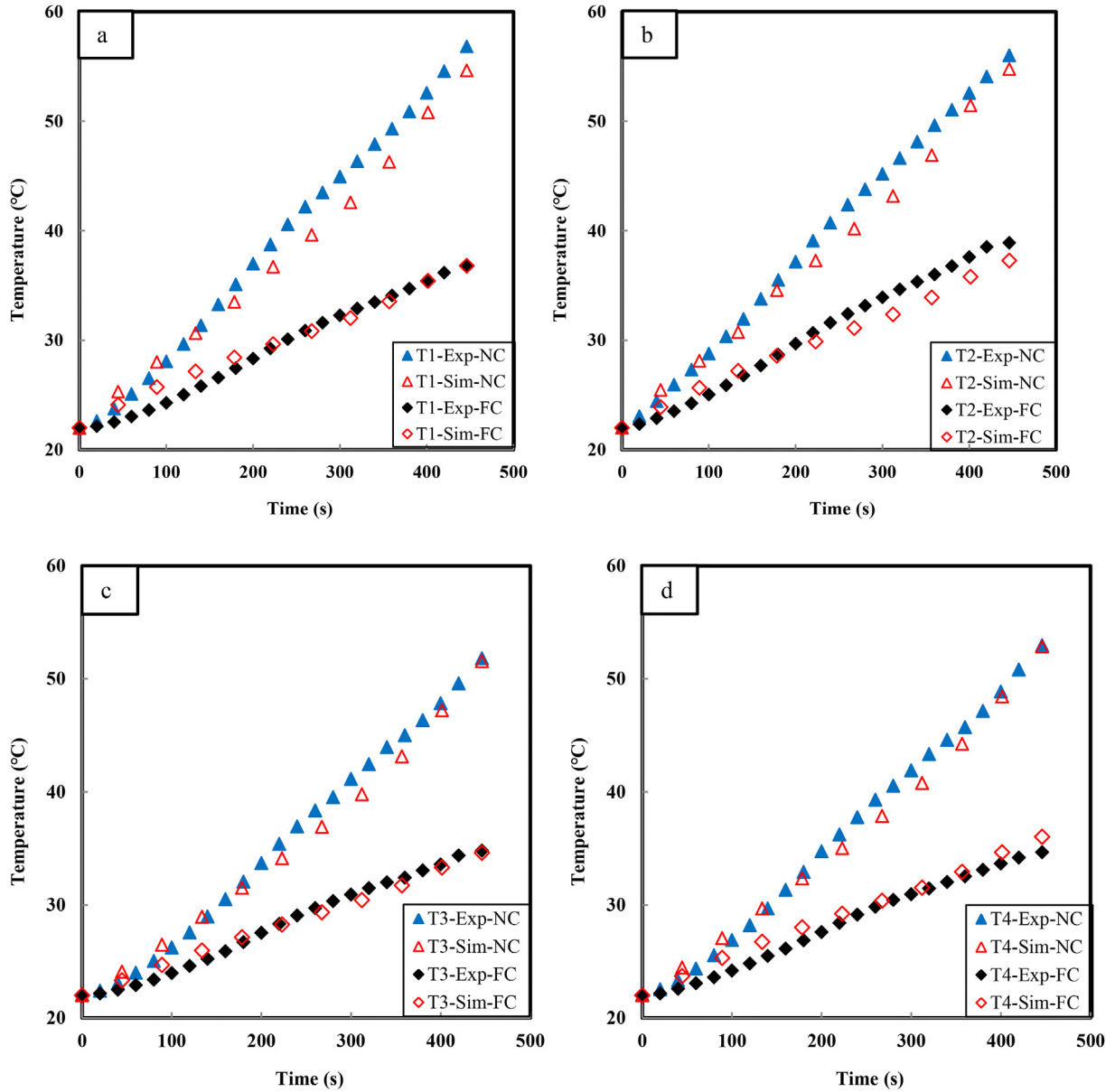
Fig. 10. Thermal model validation of forced and natural convection for (a) T$_1$, (b) T$_2$, (c) T$_3$, and (d) T$_4$ in the 8C discharging rate (Sim: Simulation, NC: Natural convection, FC: Forced convection).

$$\dot{q} = R_{tab} \cdot (I_{batt})^2 \qquad (7)$$

$$R_{tab} = \rho' \frac{l}{A} \qquad (8)$$

where I_{batt}, R_{tab}, ρ', l, and A are current, electrical resistance, resistivity, length, and the cross-section of the corresponding tab respectively. q_{Conv} represents the convective heat transfer from the cell to the ambient, which is calculated as follows:

$$q_{Conv} = hA(T_{amb} - T_{bt}) \qquad (9a)$$

where, h, A, T_{bt} and T_{amb} represent the heat transfer coefficient, cross-section area of the cell, battery and ambient temperature, respectively. The temperature transient simulation of the cell in natural and forced convection is shown in Fig. 9. In the following

simulation, the heat pipe is replaced by a solid region, and the effective thermal conductivity of components is used in the simulation [29,37,47,48].

4.2. Validation based on experimental results

To validate the numerical thermal model of the battery, the simulation and experimental results at the 8C discharging rate are compared under the natural and forced convection cooling methods. The experimental temperatures are measured by eight K-type thermocouples, as they are shown in Figs. 6a and 7a. The temperature comparison between the experimental and simulation results displays in Fig. 10. It can be seen there is an acceptable agreement between experimental and simulation results for thermocouples of T$_1$, T$_2$, T$_3$, and T$_4$.
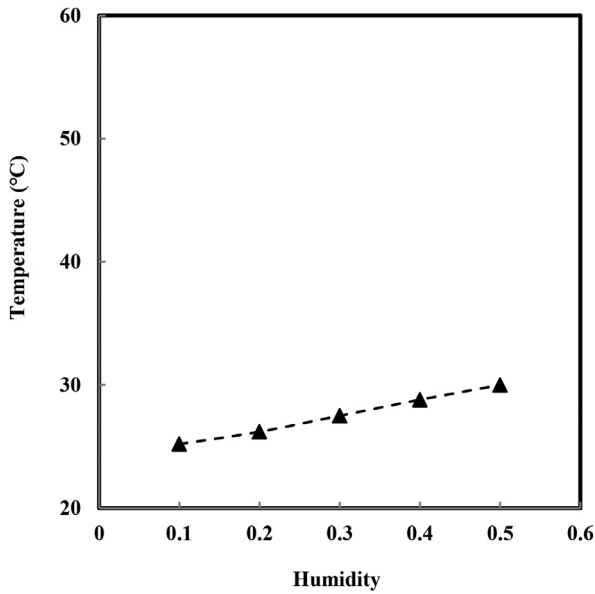
Fig. 11. Effect of the relative humidity of inlet air on cell temperature in the 8C discharging rate.
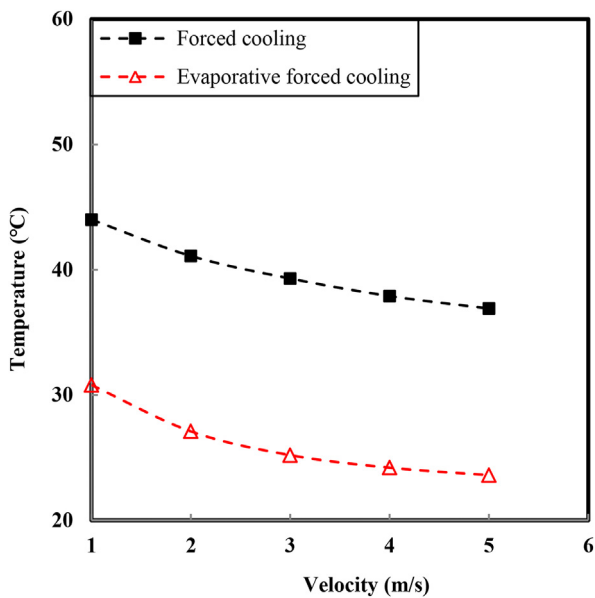

Fig. 12. Comparison of cell temperature for forced and evaporative cooling in the 8C discharging rate.

Table 2
The main properties of the module.

Parameter	Value
Number of cells in series	30
Nominal voltage of the module (V)	69
Weight (kg)	16.5
Volume (L)	7.8
Stored energy in the module (KWh)	1.6

4.3. Concept of the evaporative cooling system

4.3.1. Optimization in cell level by evaporative cooling

A test rig at a cell level is built to validate the numerical simulation results with experimental measurements. As it is approved in Fig. 10, there is an acceptable agreement between the simulation and experimental results. The evaporative cooling method is classified as a phase change cooling that wet surface absorbs heat in order to change from the liquid state to vapor state, resulting in the reduction of heat source temperature. Evaporative cooling is an efficient, economic, and energy-saving cooling method in contrast with conventional bulky liquid cooling systems [49,50]. The vaporization latent heat of the phase change process from liquid to vapor is the main advantage of evaporative cooling compare with the forced convection cooling method [51]. Evaporative cooling is a developed knowledge that has been used in industrial cooling applications such as cooling towers and gas turbines [52]. In this technology, the temperature of the heat source(condenser) is reduced by the evaporation of water from liquid to vapor. The mathematical analysis of the evaporative cooling system is presented in the following equation [53].

$$M_a dh_a = [hA(T_{amb} - T_{bt}) + K_1(W_{asw} - W_a)h_{vs}]dA \tag{9b}$$

where h_{vs}, W_{asw}, h_a and K_1 represent the enthalpy of water vapor at water surface temperature, the humidity ratio of air, the enthalpy of the air, and the mass transfer coefficient respectively. Moreover, for calculation of the evaporation heat flux equation (10) can be used as follows:

$$\dot{m}_{evap} = K(c_{sat} - c_V)M_V \tag{10}$$

where K, M_V, c_V and c_{sat} represent the evaporation rate, the molar mass of water vapor, vapor, and saturation concentration respectively [54]. The offered battery TMS depends on thin flat heat pipes, which can efficiently transfer the heat from the cells to the coolant. In the proposed cooling system, the condenser section of the heat pipes is covered by a wet surface. In fact, the phase change happens inside and outside of the heat pipes. In the proposed cooling method, the relative inlet air humidity has a direct effect on cooling performance. Fig. 11 shows the maximum temperature of the cell in different relative humidity of inlet air at an ambient temperature of 22 °C.

It is obvious that the temperature of the cell rise by increasing the relative inlet air humidity. The reason returns to the wet surface area where the evaporative cooling is happening. When the value of relative humidity increases, it can decrease the evaporation rate from the heat pipe condenser area which rises the temperature [41,55]. Therefore, 10% of relative humidity is chosen for optimization as the best cooling performance. It is necessary to mention that 10% of relative humidity is not a standard value and requires a refrigerative and/or desiccant air dryer. Fig. 12 shows the comparison of maximum cell temperature at the end of the discharging process in different air velocities and the ambient temperature of 22 °C for forced and evaporative cooling. According to Fig. 11, the relative humidity is chosen by 10% for all tests.

It can be seen that increasing the inlet velocity has a direct effect on the maximum temperature of the cell in both cooling methods. It was found that by increasing the inlet velocity the maximum temperature of the cell has been decreased from 44 °C to 36.9 °C and from 30.8 °C to 23.6 °C for forced and evaporative cooling respectively. According to the results, there is a 35.8% reduction in the maximum temperature of the cell in the inlet velocity of 3 m/s due to the effect of the evaporative cooling method. For the economical comparison maintaining the fan power at a relatively lower level at which the batteries can operate safely and reliably is more reasonable. As a result, evaporative cooling presents ideal cooling performance whereas ensuring the least amount of power consumption.
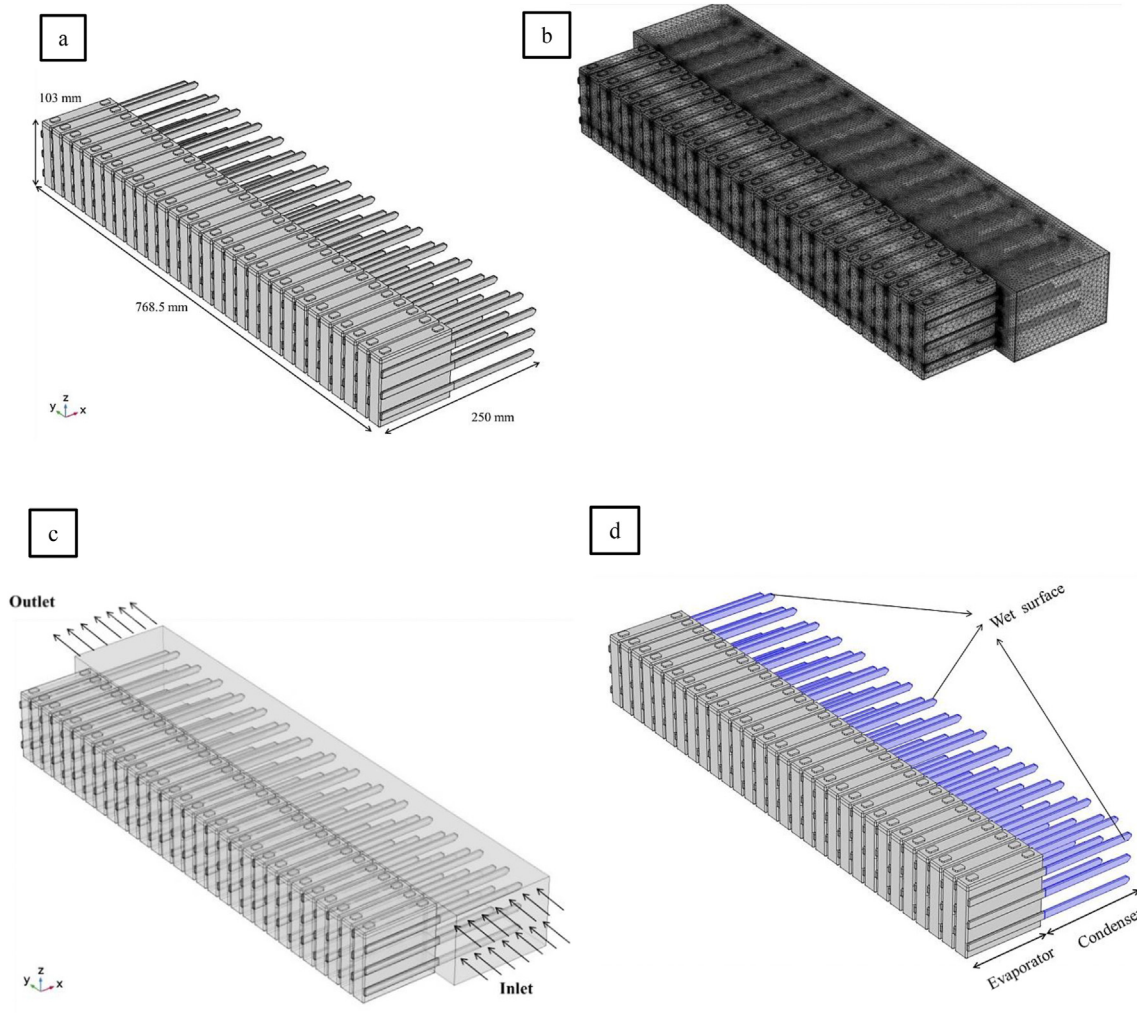
Fig. 13. (a) Schematic of the battery module, (b) mesh distribution, (c) inlet and outlet velocity of the module, and (d) wet surface area of the module in the evaporative cooling method.
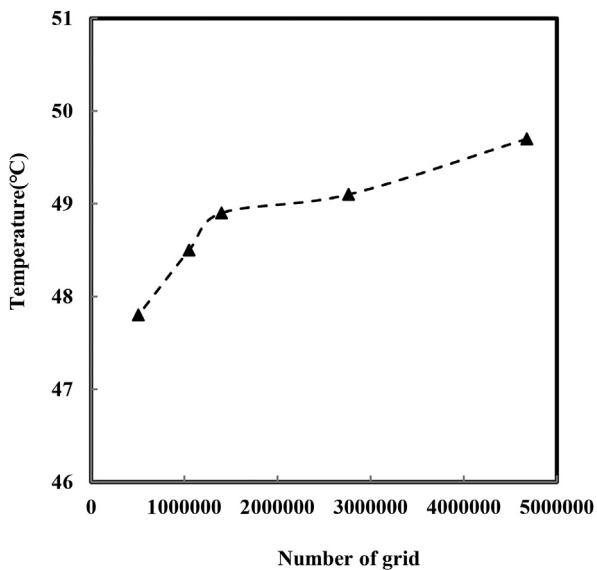

Fig. 14. Grid number independency test.

5. Performance of the thermal management methods in module level

5.1. Design of the module

5.1.1. Configuration design of the module

In this section, a module consisting of 30 cells is designed to characterize the thermal performance of the heat pipe-based air cooling system. For this aim, a 3D thermal model is developed and solved numerically by COMSOL Multiphysics® to predict the transient temperature rise of cells in the actual battery module. Battery module thermal performance is different from a single battery cell, as cells are influenced by each other during the heat transfer process. The temperature of the cells in the module is significantly affected by the cell arrangement, charge/discharge strategy, and TMS. One of the most common types of battery thermal management systems is air cooling, which has a low cost and simple structure. Several companies such as Toyota Prius, Honda Insight, Nissan, and GM, use forced convection as a thermal management system [56,57]. Air cooling owing to the low heat transfer coefficient of air is not recommended in high current and stressful conditions [58,59]. However, in the current study, the mentioned problem has been reduced using heat pipes. The main specifications of the module are given in Table 2.
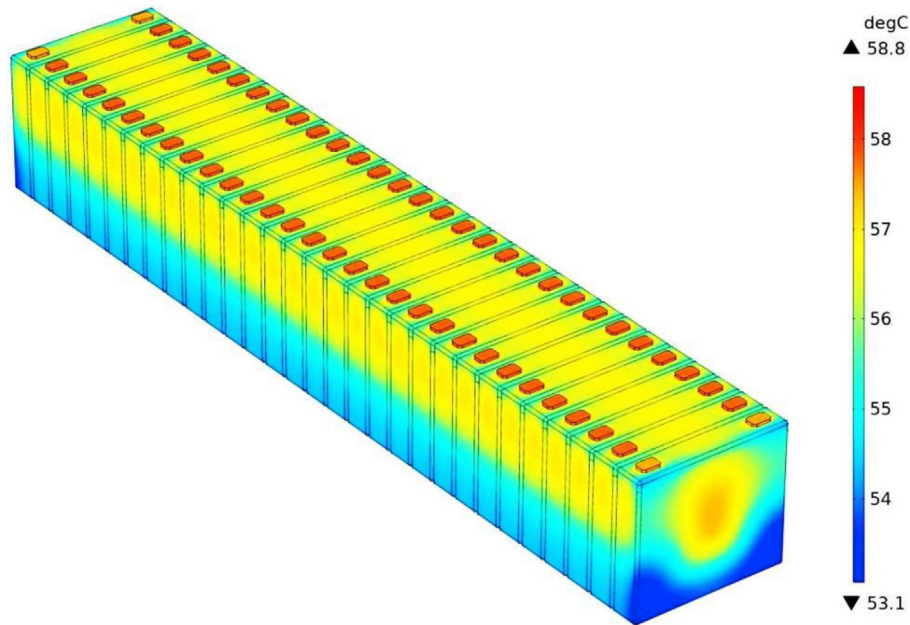
Fig. 15. Temperature contour of the module in natural convection in the 8C(184 A) discharging rate(446 s).
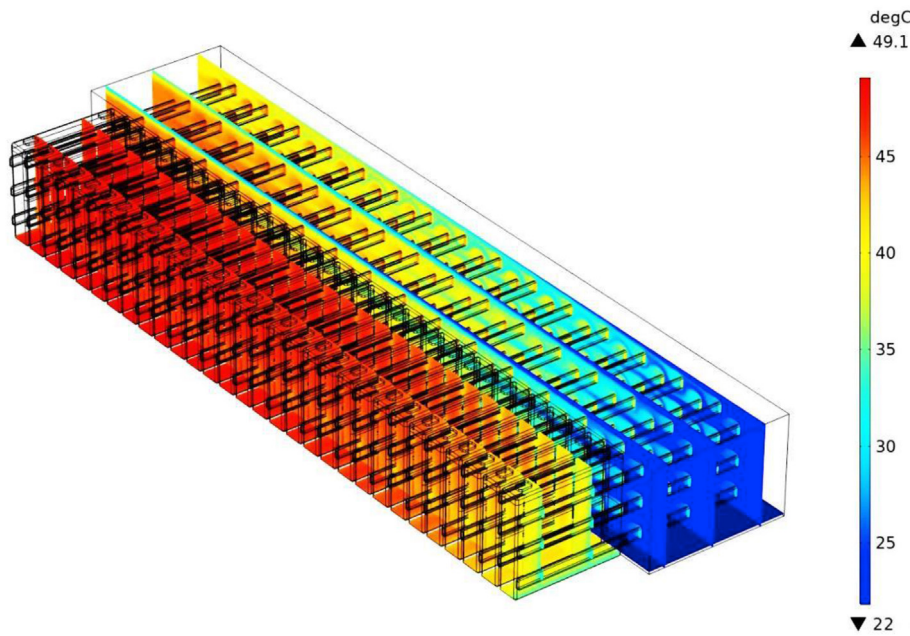

Fig. 16. Temperature contour of the module embedded with heat pipes in forced convection with an inlet velocity of 3 m/s in the 8C (184 A) discharging rate (446 s).

Fig. 13a and b shows the geometry and mesh distribution of the LTO prismatic battery module, respectively. Moreover, Fig. 13c displays the inlet and outlet air velocity of the module. In this design, the module combined with heat pipes whiles the evaporator section (115 mm) of heat pipes connected to the cells and condenser section (135 mm) of heat pipes are cooled by a cooling medium.

5.1.2. Boundary condition and mesh grid independency for module level

As it is mentioned in the cell level, the initial temperature of the battery cells, heat pipes, and the coolant are set to 22 °C. Moreover, coolant inlet velocity is set to 3 m/s, and the outlet is assumed as

the ambient pressure. The heat transfer through radiation is assumed to be negligible. The condenser section of the heat pipes is assumed to be wet for the evaporative cooling method. The 3D-thermal model is developed and solved numerically by COMSOL Multiphysics® using the heat transfer module of a commercial finite element solver, which is computed using the GMRES solver. The time step size is set on the 1 s. Besides, the grid-independent test is performed to refine the grid number while the results are not influenced by further refinement of the mesh, and the results error is kept within 5% [60]. The mesh is generated by default Physics-controlled mesh, which is an unstructured tetrahedral mesh.

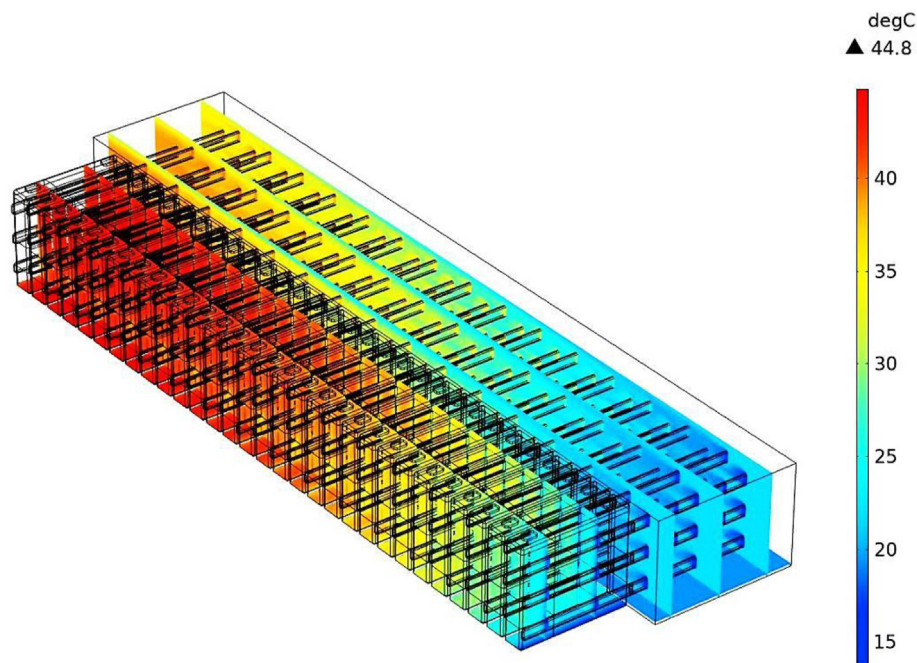Fig. 14 displays the maximum simulated temperature of the

Fig. 17. Temperature contour of the module embedded with heat pipes in evaporative cooling with an inlet velocity of 3 m/s in the 8C (184 A) discharging rate (446 s).

module by the forced cooling method to estimate the independence of the grid number. The result differs only 0.4% when the grid number varies from 2,764,662 to 4,678,590. Consequently, owing to computational time-saving, the grid number of 2,764,662 is chosen for the module simulation.

5.2. Results of the thermal management methods in module level

5.2.1. Effect of the natural convection on the module

The module temperature should be studied in natural convection conditions, to compare with the heat transfer efficiency of the heat pipe-based air cooling system and evaporative cooling method. The temperature distribution inside the module has been considered in the same initial boundary condition as the cell level. Fig. 15 shows the module which cooled through natural convection and experiences a maximum temperature of 58.8 °C. The main inability of the cooling method is the low cooling surface area and the limited thermal heat transfer of the natural air convection. The temperature distribution grows non-uniform into the module over the whole surface of the cells with more concentration in the center and top region of the cells.

5.2.2. Effect of the forced convection on the module

With the implementation of a heat pipe-based air cooling system, the maximum temperature of the module significantly decreased. At the 8C discharging rate, the maximum temperature rise decreases from 58.8 °C to 49.1 °C compared with natural convection. As shown in Fig. 16 when the module is subjected to cool by forced convection and heat pipes, the internal temperature of the battery module is controlled to below 49 °C at the end of the discharging process. This suggests that the present cooling system decreased the temperature by 16.4% however, it roughly meets the requirements of battery thermal management. To further improve the performance of the present cooling system and to meet the tight requirement on maintaining the module temperature in a safe range [61] several scenarios like evaporative cooling, increasing the flow rate, or decreasing the airflow temperature could be implemented.
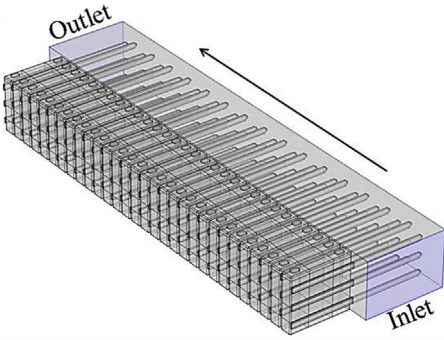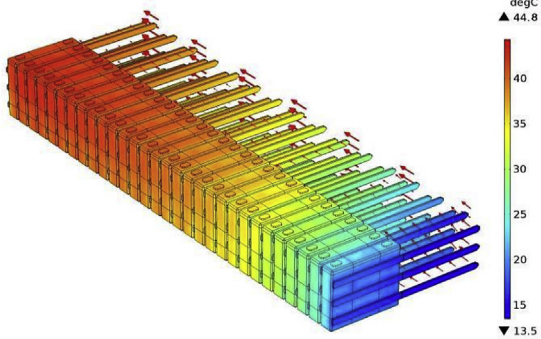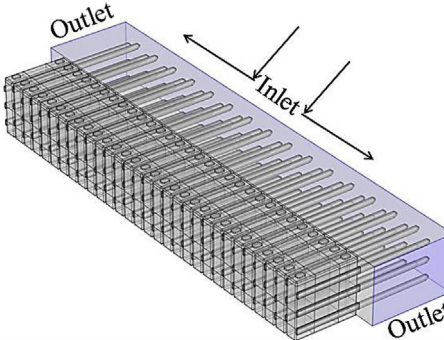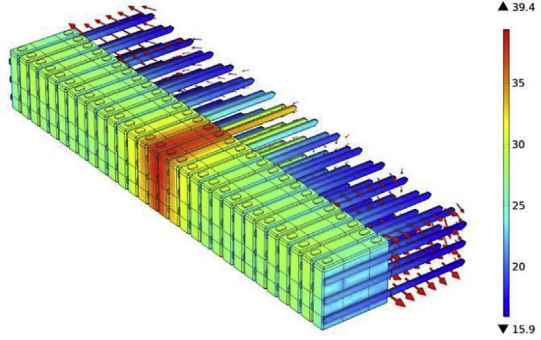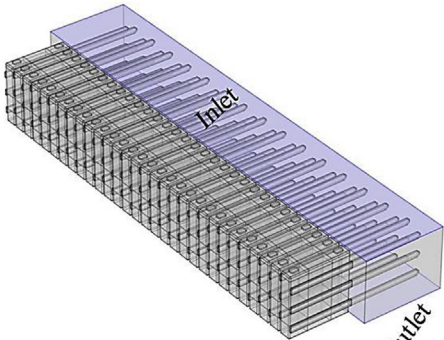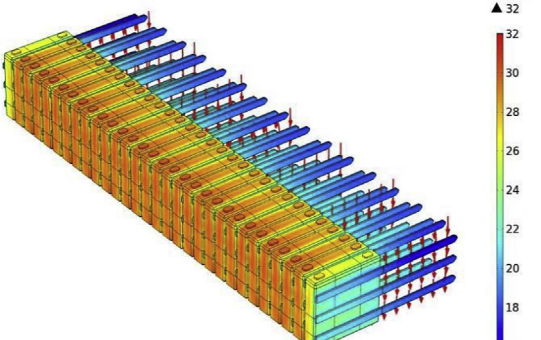
5.2.3. Effect of the evaporative cooling on the module

This section represents a transient simulation to estimate the temperature rise of the battery module under the 8C discharging rate and with inlet air temperature and velocity of 22 °C and 3 m/s, respectively. According to Fig. 17, the maximum temperature of the module reached 44.8 °C. As compared to the temperature of the module with the natural cooling system, the overall surface temperature of the module is reduced by 23.8% using the evaporative cooling method. The simulation results further confirm that evaporative cooling is a possible cooling method for the development of the Li-ion battery module/pack TMS.

5.2.3.1. *Investigation of temperature uniformity in the evaporative cooling on the module.* In the last section, evaporative cooling is introduced as a possible cooling method that keeps the maximum temperature of the module at 44.8 °C. However, the temperature uniformity is not suitable and the cell temperatures increase from the inlet to the outlet. Therefore, the optimization of the inlet and outlet of the airflow is done to improve temperature uniformity and reduce maximum module temperature. Table 3 shows the battery TMS with inlet and outlet optimization in three different cases with an inlet velocity of 3 m/s. Case 1 represents the existing model which suffers from temperature uniformity due to the position of the inlet and outlet and a large number of cells in the module. Case 2 displays the inlet in front of the module with two outlets from the sides. It can be seen, the maximum temperature has been decreased. However, there is a temperature increase in the middle of the module owing to the tendency of the airflow to the outlets. In case 3 the inlet is located at the top and the outlet located on the downside of the module. The maximum temperature of the module has been decreased by 26.8 °C which shows a 45.5% reduction. Moreover, there is an acceptable temperature uniformity inside the module.

Table 3
Battery TMS with inlet and outlet optimization.

Power Consumption	Inlet and outlet position	Temperature distribution
12 W		
60 W		
60 W		

6. Comparison of the proposed cooling system in the cell and module levels

6.1. Cell level

The thermal performance of Li-ion batteries varies with time at the cell and module level. Therefore, the ability of a TMS to preserve the cell/module temperature under different working conditions is vital. In order to investigate the efficiency of the evaporative cooling method and compare the results with forced and natural convection, the average temperature of the cell in different time steps is shown in Fig. 18. In the baseline condition, the single-cell experienced dramatic temperature growth and reached 53.66 °C. The temperature of the cell has been decreased significantly by equipping the heat pipe-based air cooling system and reached 36.88 °C. The evaporative cooling system shows a perfect cooling performance and maintains the temperature of the cell in the range of 22 °C. It is obvious that at the primary stages of discharge, the temperature of the cell cooled and experiences slight temperature drops owing to the evaporation effect which improves convective heat dissipation.

6.2. Module-level

According to Fig. 19, for natural convection, the module level experienced a more severe temperature increase and reached 56.6 °C. The average temperature of the module increased from 22 °C to 56.6 °C which shows a 61.1% increase. To control and decrease the heat accumulation of the module the heat pipe-based air cooling system is carried out on the battery module. The temperature of the module has been decreased to 45.61 °C by the mentioned cooling system. The evaporative cooling system shows a reasonable cooling performance and decreased the average temperature of the module to 37.92 °C.
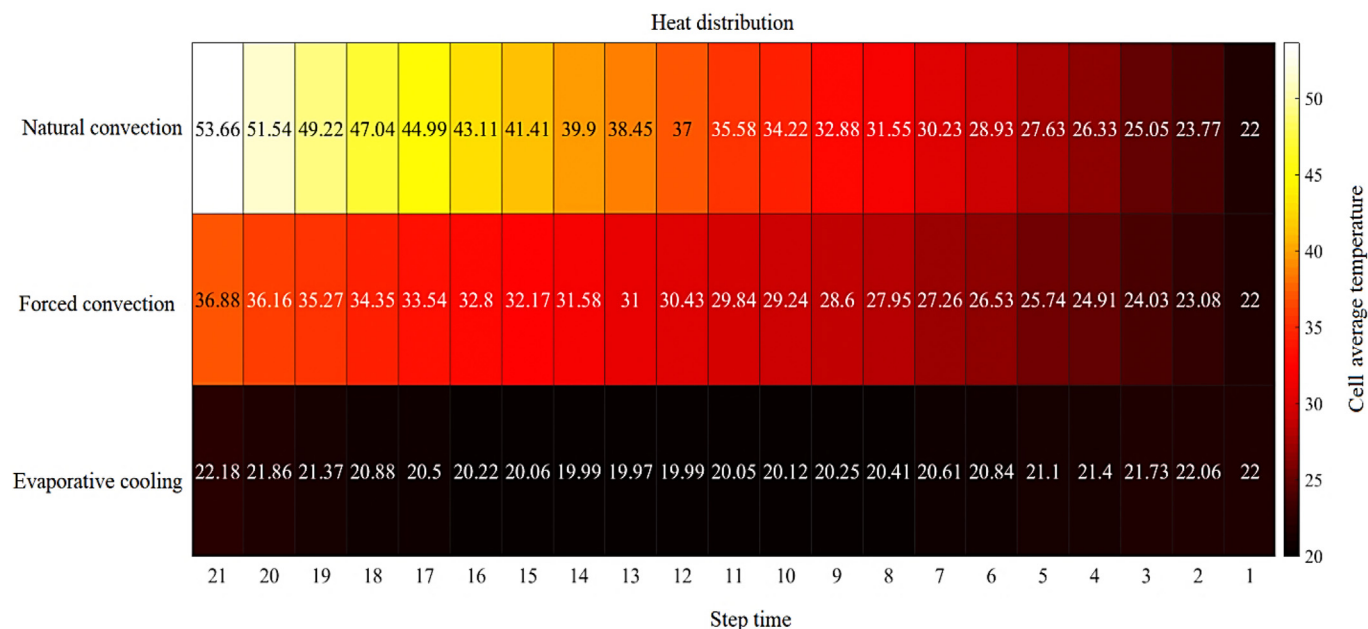
Fig. 18. Comparison of the average cell temperature for natural, forced, and evaporative cooling methods in the 8C discharging rate.
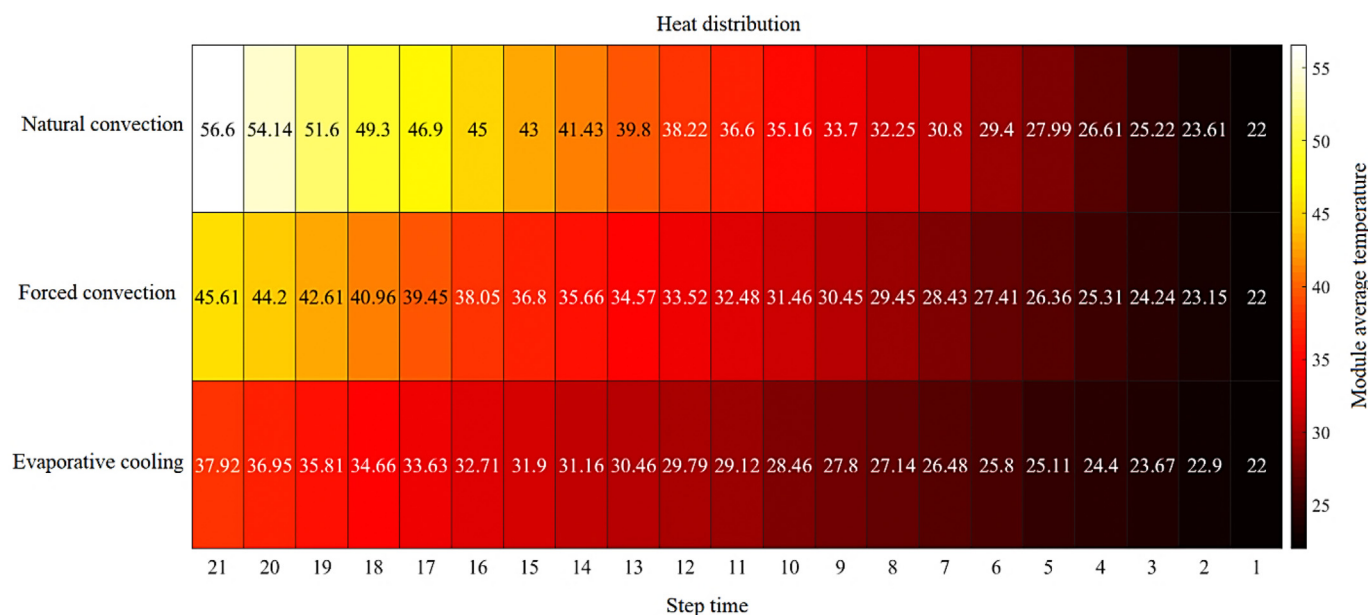

Fig. 19. Comparison of the average module temperature for natural, forced, and evaporative cooling methods in the 8C discharging rate.

As it was proved the forced convection and evaporative cooling are successful cooling systems for the module level in the 8C discharging rate. Therefore, the investigation of different inlet velocity effects on the maximum temperature of the module is an important item. Fig. 20 shows that increasing the inlet velocity from 1 m/s to 7 m/s has a direct consequence on the maximum temperature of the module in both cooling methods. The trend of the maximum temperature of the module has been decreased from 51 °C to 46.7 °C and from 47.6 °C to 40.3 °C for forced and evaporative cooling respectively. According to the results, there is an average of 10% reduction in the maximum temperature of the module due to the effect of the evaporative cooling method. The present study shows that the evaporative cooling method can preserve the

maximum temperature of the module in a safe range (25−40 °C) with an inlet velocity of 7 m/s.

7. Conclusion

The current study experimentally and numerically investigated a heat pipe-based air cooling TMS for the LTO battery cell/module. A number of optimization scenarios were developed. In the first scenario, the temperature of the cell was considered experimentally in the lack and presence of natural convection. In the second scenario, the effect of the heat pipe-based air cooling system was investigated. It was found that the average cell temperature reached from 54.3 °C to 35.9 °C, which showed a 33.7% reduction.
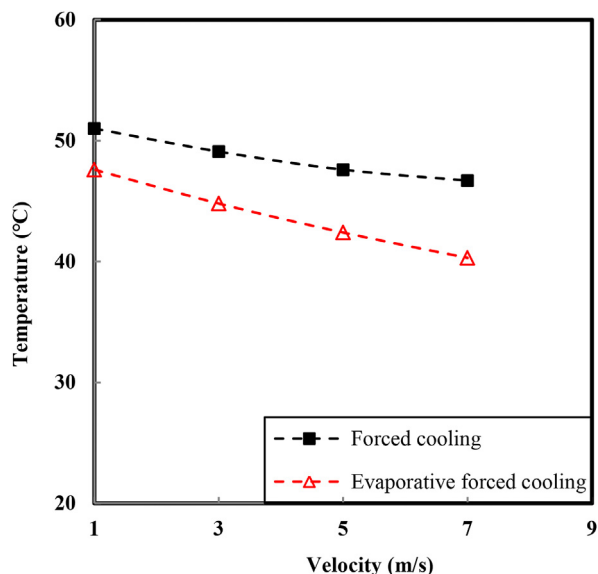
Fig. 20. Comparison of the module temperature for forced and evaporative cooling in different inlet velocities at the 8C discharging rate.

Finally, in the third scenario, the effect of evaporative cooling was considered for the cell/module level. According to the results, there was a 35.8% reduction in the maximum temperature of the cell due to the effect of the evaporative cooling method. Moreover, the maximum temperature of the battery module was reduced by 23.8% compared with the natural convection.

Credit author contribution statement

Hamidreza Behi: Conceptualization, Methodology, Software, Experiment, Validation, Investigation, Data curation, Writing − original draft., Danial Karimi: Software, Investigation, Validation., Joris Jaguemont: Methodology, Writing − review & editing., Foad Heidari Gandoman: Writing − review & editing., Theodoros Kalogiannis: Writing, Data curation, Visualization., Maitane Berecibar: Review & editing., Joeri Van Mierlo: Supervision.

Declaration of competing interest

The authors declare that they have no known competing financial interests or personal relationships that could have appeared to influence the work reported in this paper.

Acknowledgment

References

[1] Yang W, Zhou F, Zhou H, Wang Q, Kong J. Thermal performance of cylindrical Lithium-ion battery thermal management system integrated with mini-channel liquid cooling and air cooling. Appl Therm Eng 2020:115331. https://doi.org/10.1016/J.APPLTHERMALENG.2020.115331.

[2] Chen F, Huang R, Wang C, Yu X, Liu H, Wu Q, Qian K, Bhagat R. Air and PCM cooling for battery thermal management considering battery cycle life. Appl Therm Eng 2020;173:115154. https://doi.org/10.1016/J.APPLTHERMALENG.2020.115154.

[3] Lei S, Shi Y, Chen G. A lithium-ion battery-thermal-management design based on phase-change-material thermal storage and spray cooling. Appl Therm Eng 2020;168:114792. https://doi.org/10.1016/J.APPLTHERMALENG.2019.114792.

[4] Xu X, Li W, Xu B, Qin J. Numerical study on a water cooling system for prismatic LiFePO4 batteries at abused operating conditions. Appl Energy 2019;250:404−12. https://doi.org/10.1016/J.APENERGY.2019.04.180.

[5] Khaleghi S, Karimi D, Beheshti SH, Hosen MS, Behi H, Berecibar M, Van Mierlo J. Online health diagnosis of lithium-ion batteries based on nonlinear autoregressive neural network. Appl Energy 2021;282:116159. https://doi.org/10.1016/j.apenergy.2020.116159.

[6] Cao J, Ling Z, Fang X, Zhang Z. Delayed liquid cooling strategy with phase change material to achieve high temperature uniformity of Li-ion battery under high-rate discharge. J Power Sources 2020;450:227673. https://doi.org/10.1016/J.JPOWSOUR.2019.227673.

[7] Raijmakers LHJ, Danilov DL, Eichel R-A, Notten PHL. A review on various temperature-indication methods for Li-ion batteries. Appl Energy 2019;240:918−45. https://doi.org/10.1016/j.apenergy.2019.02.078.

[8] Saw LH, Ye Y, Tay AAO, Chong WT, Kuan SH, Yew MC. Computational fluid dynamic and thermal analysis of Lithium-ion battery pack with air cooling. Appl Energy 2016;177:783−92. https://doi.org/10.1016/j.apenergy.2016.05.122.

[9] Behi H, Behi M, Karimi D, Jaguemont J, Ghanbarpour M, Behnia M, Berecibar M, Van Mierlo J. Heat pipe air-cooled thermal management system for lithium-ion batteries: high power applications. Appl Therm Eng 2020:116240. https://doi.org/10.1016/j.applthermaleng.2020.116240.

[10] Park H. A design of air flow configuration for cooling lithium ion battery in hybrid electric vehicles. J Power Sources 2013;239:30−6. https://doi.org/10.1016/J.JPOWSOUR.2013.03.102.

[11] Safdari M, Ahmadi R, Sadeghzadeh S. Numerical investigation on PCM encapsulation shape used in the passive-active battery thermal management. Energy 2020;193:116840. https://doi.org/10.1016/J.ENERGY.2019.116840.

[12] Zhou H, Zhou F, Zhang Q, Wang Q, Song Z. Thermal management of cylindrical lithium-ion battery based on a liquid cooling method with half-helical duct. Appl Therm Eng 2019;162:114257. https://doi.org/10.1016/J.APPLTHERMALENG.2019.114257.

[13] Karimi D, Behi H, Jaguemont J, El Baghdadi M, Van Mierlo J, Hegazy O. Thermal concept design of MOSFET power modules in inverter subsystems for electric vehicles. 2019.

[14] Behi M, Mirmohammadi SA, Ghanbarpour M, Behi H, Palm B. Evaluation of a novel solar driven sorption cooling/heating system integrated with PCM storage compartment. Energy 2018;164:449−64. https://doi.org/10.1016/J.ENERGY.2018.08.166.

[15] Ling Z, Cao J, Zhang W, Zhang Z, Fang X, Gao X. Compact liquid cooling strategy with phase change materials for Li-ion batteries optimized using response surface methodology. Appl Energy 2018;228:777−88. https://doi.org/10.1016/j.apenergy.2018.06.143.

[16] Gandoman FH, Behi H, Berecibar M, Jaguemont J, Aleem SHEA, Behi M, Van Mierlo J. Chapter 16 - reliability evaluation of Li-ion batteries for electric vehicles applications from the thermal perspectives. In: Zobaa AF, Abdel Aleem SHE, editors. Uncertainties mod. Power syst. Academic Press; 2021. p. 563−87. https://doi.org/10.1016/B978-0-12-820491-7.00016-5.

[17] Zhu Z, Wu X, Zhang H, Guo Y, Wu G. Multi-objective optimization of a liquid cooled battery module with collaborative heat dissipation in both axial and radial directions. Int J Heat Mass Tran 2020;155:119701. https://doi.org/10.1016/j.ijheatmasstransfer.2020.119701.

[18] Kong D, Peng R, Ping P, Du J, Chen G, Wen J. A novel battery thermal management system coupling with PCM and optimized controllable liquid cooling for different ambient temperatures. Energy Convers Manag 2020;204:112280. https://doi.org/10.1016/J.ENCONMAN.2019.112280.

[19] Cao J, Luo M, Fang X, Ling Z, Zhang Z. Liquid cooling with phase change materials for cylindrical Li-ion batteries: an experimental and numerical study. Energy 2020;191:116565. https://doi.org/10.1016/J.ENERGY.2019.116565.

[20] Karimi D, Behi H, Hosen MS, Jaguemont J, Berecibar M, Van Mierlo J. A compact and optimized liquid-cooled thermal management system for high power lithium-ion capacitors. Appl Therm Eng 2021;185:116449. https://doi.org/10.1016/j.applthermaleng.2020.116449.

[21] Jilte RD, Kumar R, Ahmadi MH, Chen L. Battery thermal management system employing phase change material with cell-to-cell air cooling. Appl Therm Eng 2019;161:114199. https://doi.org/10.1016/j.applthermaleng.2019.114199.

[22] Akinlabi AAH, Solyali D. Configuration, design, and optimization of air-cooled battery thermal management system for electric vehicles: a review. Renew Sustain Energy Rev 2020;125:109815. https://doi.org/10.1016/j.rser.2020.109815.

[23] Chen K, Song M, Wei W, Wang S. Design of the structure of battery pack in parallel air-cooled battery thermal management system for cooling efficiency improvement. Int J Heat Mass Tran 2019;132:309−21. https://doi.org/10.1016/j.ijheatmasstransfer.2018.12.024.

[24] Behi H, Karimi D, Jaguemont J, Gandoman FH, Khaleghi S, Van Mierlo J, Berecibar M. Aluminum heat sink assisted air-cooling thermal management system for high current applications in electric vehicles. AEIT int. Conf. Electr. Electron. Technol. Automot. AEIT AUTOMOTIVE); 2020. p. 1−6. 2020.

[25] Fathabadi H. A novel design including cooling media for Lithium-ion batteries pack used in hybrid and electric vehicles. J Power Sources 2014;245:495−500. https://doi.org/10.1016/J.JPOWSOUR.2013.06.160.

[26] Behi H, Ghanbarpour M, Behi M. Investigation of PCM-assisted heat pipe for

electronic cooling. Appl Therm Eng 2017;127:1132–42. https://doi.org/10.1016/J.APPLTHERMALENG.2017.08.109.

[27] Karimi D, Behi H, Jaguemont J, Sokkeh MA, Kalogiannis T, Hosen MS, Berecibar M, Van Mierlo J. Thermal performance enhancement of phase change material using aluminum-mesh grid foil for lithium-capacitor modules. J. Energy Storage. 2020;30:101508. https://doi.org/10.1016/j.est.2020.101508.

[28] Ling Z, Wang F, Fang X, Gao X, Zhang Z. A hybrid thermal management system for lithium ion batteries combining phase change materials with forced-air cooling. Appl Energy 2015;148:403–9. https://doi.org/10.1016/J.APENERGY.2015.03.080.

[29] Behi H. Experimental and numerical study on heat pipe assisted PCM storage system. 2015.

[30] Mirmohammadi S, Behi M. Investigation on thermal conductivity, viscosity and stability of nanofluids. 2012. p. 140. 537164, http://kth.diva-portal.org/smash/record.jsf?pid=diva2.

[31] Behi M, Shakorian-poor M, Mirmohammadi SA, Behi H, Rubio JI, Nikkam N, Farzaneh-Gord M, Gan Y, Behnia M. Experimental and numerical investigation on hydrothermal performance of nanofluids in micro-tubes. Energy 2020;193:116658. https://doi.org/10.1016/J.ENERGY.2019.116658.

[32] Jaguemont J, Karimi D, Van Mierlo J. Optimal passive thermal management of lithium-ion capacitors for automotive applications. 2019. p. 1–8.

[33] Heyhat MM, Mousavi S, Siavashi M. Battery thermal management with thermal energy storage composites of PCM, metal foam, fin and nanoparticle. J. Energy Storage. 2020;28:101235. https://doi.org/10.1016/J.EST.2020.101235.

[34] Zhao J, Lv P, Rao Z. Experimental study on the thermal management performance of phase change material coupled with heat pipe for cylindrical power battery pack. Exp Therm Fluid Sci 2017;82:182–8. https://doi.org/10.1016/J.EXPTHERMFLUSCI.2016.11.017.

[35] Ye Y, Saw LH, Shi Y, Tay AAO. Numerical analyses on optimizing a heat pipe thermal management system for lithium-ion batteries during fast charging. Appl Therm Eng 2015;86:281–91. https://doi.org/10.1016/J.APPLTHERMALENG.2015.04.066.

[36] Feng L, Zhou S, Li Y, Wang Y, Zhao Q, Luo C, Wang G, Yan K. Experimental investigation of thermal and strain management for lithium-ion battery pack in heat pipe cooling. J. Energy Storage. 2018;16:84–92. https://doi.org/10.1016/J.EST.2018.01.001.

[37] Behi H, Karimi D, Behi M, Ghanbarpour M, Jaguemont J, Akbarzadeh Sokkeh M, Heidari Gandoman F, Berecibar M, Van Mierlo J. A new concept of thermal management system in Li-ion battery using air cooling and heat pipe for electric vehicles. Appl Therm Eng 2020:115280. https://doi.org/10.1016/J.APPLTHERMALENG.2020.115280.

[38] Dan D, Yao C, Zhang Y, Zhang H, Zeng Z, Xu X. Dynamic thermal behavior of micro heat pipe array-air cooling battery thermal management system based on thermal network model. Appl Therm Eng 2019;162:114183. https://doi.org/10.1016/J.APPLTHERMALENG.2019.114183.

[39] Zhao R, Gu J, Liu J. An experimental study of heat pipe thermal management system with wet cooling method for lithium ion batteries. J Power Sources 2015;273:1089–97. https://doi.org/10.1016/J.JPOWSOUR.2014.10.007.

[40] Tran T-H, Harmand S, Desmet B, Filangi S. Experimental investigation on the feasibility of heat pipe cooling for HEV/EV lithium-ion battery. Appl Therm Eng 2014;63:551–8. https://doi.org/10.1016/J.APPLTHERMALENG.2013.11.048.

[41] Zhao R, Liu J, Gu J, Zhai L, Ma F. Experimental study of a direct evaporative cooling approach for Li-ion battery thermal management. Int J Energy Res 2020;44:6660–73. https://doi.org/10.1002/er.5402.

[42] Behi H, Karimi D, Behi M, Jaguemont J, Ghanbarpour M, Behnia M, Berecibar M, Van Mierlo J. Thermal management analysis using heat pipe in the high current discharging of lithium-ion battery in electric vehicles. J. Energy Storage 2020;32:101893. https://doi.org/10.1016/j.est.2020.101893.

[43] Sheikholeslami M, Ganji DD. Heat transfer improvement in a double pipe heat exchanger by means of perforated turbulators. Energy Convers Manag 2016;127:112–23. https://doi.org/10.1016/J.ENCONMAN.2016.08.090.

[44] Sheikholeslami M, Ganji DD. Heat transfer enhancement in an air to water heat exchanger with discontinuous helical turbulators; experimental and numerical studies. Energy 2016;116:341–52. https://doi.org/10.1016/J.ENERGY.2016.09.120.

[45] Nemati H, Moradaghay M, Shekoohi SA, Moghimi MA, Meyer JP. Natural convection heat transfer from horizontal annular finned tubes based on modified Rayleigh Number. Int Commun Heat Mass Tran 2020;110:104370. https://doi.org/10.1016/j.icheatmasstransfer.2019.104370.

[46] Kalogiannis T, Hosen MS, Sokkeh MA, Goutam S, Jaguemont J, Jin L, Qiao G, Berecibar M, Van Mierlo J. Comparative study on parameter identification methods for dual-polarization lithium-ion equivalent circuit model. Energies 2019;12:1–37. https://doi.org/10.3390/en12214031.

[47] Ghanbarpour M, Khodabandeh R. Entropy generation analysis of cylindrical heat pipe using nanofluid. Thermochim Acta 2015;610:37–46. https://doi.org/10.1016/j.tca.2015.04.028.

[48] Elnaggar MHA, Abdullah MZ, Raj S, Munusamy R. Experimental and numerical studies of finned L-shape heat pipe for notebook-PC cooling. IEEE Trans Compon Packag Manuf Technol 2013;3:978–88. https://doi.org/10.1109/TCPMT.2013.2245944.

[49] Jiang Y, Zheng Q, Dong P, Yao J, Zhang H, Gao J. Conjugate heat transfer analysis of leading edge and downstream mist–air film cooling on turbine vane. Int J Heat Mass Tran 2015;90:613–26. https://doi.org/10.1016/j.ijheatmasstransfer.2015.07.005.

[50] Xuan YM, Xiao F, Niu XF, Huang X, Wang SW. Research and application of evaporative cooling in China: a review (I) – Research. Renew Sustain Energy Rev 2012;16:3535–46. https://doi.org/10.1016/j.rser.2012.01.052.

[51] Howes JC, Levett DB, Wilson ST, Marsala J, Saums DL. Cooling of an IGBT drive system with vaporizable dielectric fluid (VDF)," 2008 twenty-fourth annual IEEE semiconductor thermal measurement and management symposium. San Jose, CA. 2008 [n.d.)].

[52] Sun Y, Guan Z, Gurgenci H, Wang J, Dong P, Hooman K. Spray cooling system design and optimization for cooling performance enhancement of natural draft dry cooling tower in concentrated solar power plants. Energy 2019;168: 273–84. https://doi.org/10.1016/j.energy.2018.11.111.

[53] El-Ladan AD, Haas OCL. Fan-pad evaporative battery cooling for hybrid electric vehicle thermal management. IET Conf. Publ 2015. https://doi.org/10.1049/cp.2015.0901. 2015.

[54] Wickert D, Prokop G. Simulation of water evaporation under natural conditions—a state-of-the-art overview. Exp. Comput. Multiph. Flow 2020:2. https://doi.org/10.1007/s42757-020-0071-5.

[55] Terekhov VI, Gorbachev MV, Khafaji HQA. Simulation for evaporative cooling in partially wetted plate heat mass exchanger. IOP Publishing J Phys Conf 2018;1105(1) [n.d.].

[56] Kelly KJ, Mihalic M, Zolot M. Battery usage and thermal performance of the Toyota Prius and Honda Insight during chassis dynamometer testing. Proc. Annu. Batter. Conf. Appl. Adv. 2002:247–52. https://doi.org/10.1109/BCAA.2002.986408. 2002-Janua.

[57] M M, Kelly MZKJ. Battery usage and thermal performance of the Toyota Prius and Honda Insight during chassis dynamometer testing. Seventeenth annu. Batter. Conf. Appl. Adv. Proc. Conf. (Cat. No.02TH8576). 2002. p. 247–52. Long Beach, CA, USA[n.d.].

[58] Pesaran AA. Battery thermal models for hybrid vehicle simulations. J Power Sources 2002;110:377–82. https://doi.org/10.1016/S0378-7753(02)00200-8.

[59] Pesaran A. Battery thermal management in EVs and HEVs : issues and solutions. Adv. Automot. Batter. Conf. 2001:10.

[60] Ye Y, Shi Y, Saw LH, Tay AAO. Performance assessment and optimization of a heat pipe thermal management system for fast charging lithium ion battery packs. Int J Heat Mass Tran 2016;92:893–903. https://doi.org/10.1016/J.IJHEATMASSTRANSFER.2015.09.052.

[61] Bandhauer TM, Garimella S, Fuller TF. A critical review of thermal issues in lithium-ion batteries. J Electrochem Soc 2011;158. https://doi.org/10.1149/1.3515880.